A Planar High-gain Circularly Polarized Dipole Antenna Based on PRAMC for 2.45 GHz ISM Band

Xinhui Yang[1], Yizheng Ma[1], Ze Chen[1], Yuan Li[1], Hua Chen[1], Qing Fang[1, 2], Anneng Yang[1], and Song Feng[3]

[1] Faculty of Science, Kunming University of Science and Technology, Kunming, Yunnan, 650500, China
[2] Shaanxi Institute of Advanced Oeic Technologies Co.,Ltd., Xi'an, Shaanxi, 710119, China
[3] School of Science, Xi'an Polytechnic University, Xi'an, Shaanxi, 710048, China

Corresponding author: Hua Chen (e-mail: cherrychen40600@163.com).

ABSTRACT This paper presents a novel planar circularly polarized (CP) dipole antenna for 2.45 GHz ISM band wireless communications based on a polarization rotation artificial magnetic conductor (PRAMC). The design evolution begins with a linearly polarized (LP) dipole antenna, followed by the dipole antenna loaded with a 2×2 AMC array, and culminates in the proposed CP dipole antenna incorporating a 2×2 PRAMC array. Unlike conventional AMC arrays that only enhance gain, the proposed PRAMC array can convert LP radiation to CP radiation and further enhance the gain of the dipole antenna. Measured results indicate that the proposed antenna has the −10 dB impedance bandwidth (BW) of 29.8% (2.21–2.94 GHz), the 3 dB axial ratio (AR) BW of 7.0% (2.35–2.52 GHz), a peak gain of 7.01 dBi, indicating left-hand CP (LHCP) at 2.45 GHz. Finally, the experimental results validate that the proposed PRAMC can convert a low-gain LP dipole antenna into a high-gain CP dipole antenna.

INDEX TERMS High gain, circular polarized (CP), dipole antenna, polarization rotation artificial magnetic conductor (PRAMC)

I. INTRODUCTION

With the rapid development of wireless communication technologies, particularly the expanding applications in key areas such as 5G/6G communications, satellite communications, the Internet of Things (IoT), and radar systems, modern wireless applications have imposed increasingly stringent and diverse requirements on antenna performance. Traditional linearly polarized (LP) antennas, such as dipole antennas, have long held a significant position in antenna engineering due to their simple structure, stable radiation performance, and ease of fabrication [1-3]. However, these antennas can only radiate LP waves, with a fixed electric field vector aligned with the antenna axis. Moreover, their omnidirectional radiation characteristics can lead to energy dispersion and low gain [4]. While suitable for wide-area coverage, they struggle to meet the demands of directional communication.

Among various types of antennas, circularly polarized (CP) antennas have become an indispensable component in modern systems due to their ability to effectively mitigate multipath effects, enhance signal reception stability, and adapt well to magnetoelectric (ME) waves of arbitrary polarization directions [5-8]. Compared to LP dipole antennas, CP dipole antennas can effectively reduce signal phase distortion and attenuation while enhancing anti-interference capabilities, making them promising for applications in positioning systems, satellite communications, and other fields. However, to achieve circular polarization, dipoles typically need to be combined with magnetic dipoles to form ME dipoles, such as Cross dipole [9-10], Substrate Integrated Waveguide (SIW) [11], complementary ME dipole [12]. These methods may result in the CP dipole antennas with complex structural design, low gain, relatively narrow −10 dB impedance BW and 3 dB AR BW at 2.45 GHz ISM band, as well as increase the manufacturing cost, limiting the application in modern communications systems.

In recent years, to overcome the above limitations, researchers have actively explored new design strategies for high-gain and circularly polarized antennas. Among these, the artificial magnetic conductor (AMC) structure, as an important electromagnetic metasurface technology, has been widely introduced [13]. The AMC structure provides in-phase reflection characteristics within a specific frequency band, with its reflection phase varying around 0°, thereby effectively suppressing surface wave propagation, reducing antenna profile height, and increasing gain [14-16]. This makes it highly suitable for the urgent demands of miniaturization and integration in modern communication devices. The polarization rotation artificial magnetic conductor (PRAMC), as a special type of AMC, inherits the fundamental properties of high impedance, and in-phase reflection. Through specific unit design, it can decompose an incident LP wave into two orthogonal components with equal amplitude and a 90° phase difference, thereby enabling LP to CP conversion without complex antenna structures [17-19].

Building on previous work [20-21], which presented the ME dipole antenna loaded with segmented ring with high

FBR and LP radiation, but lower gain, thus this work seeks to overcome its limitations in gain and polarization performance. Based on previous structure, a planar CP dipole antenna is proposed by utilizing PRAMC. The uniqueness of the proposed design lies in leveraging the polarization rotation and phase manipulation capabilities of PRAMC. The PRAMC can enable LP to CP conversion. The paper is organized as follows: Section II proposes a dipole antenna; Section III presents the complete design process from a LP dipole antenna loaded with AMC to a CP dipole antenna loaded with PRAMC, and provides a comparative analysis of their performance; Section IV presents the experimental validation results. Finally, Section V concludes this paper.

II. DESIGN AND ANALYSIS OF DIPOLE ANTENNA

Figure 1 shows a schematic diagram of the initial dipole antenna structure. Specifically, a T-shaped dipole is printed on the top surface of FR4 substrate (ε_r = 4.4, tan δ = 0.02), with a slot etched at its center. A planar L-shaped balun feed line is loaded on the bottom surface to feed the antenna, forming a dipole antenna. The overall dimensions are 70 mm × 70 mm × 0.8 mm, with detailed dimensions provided in Table I.

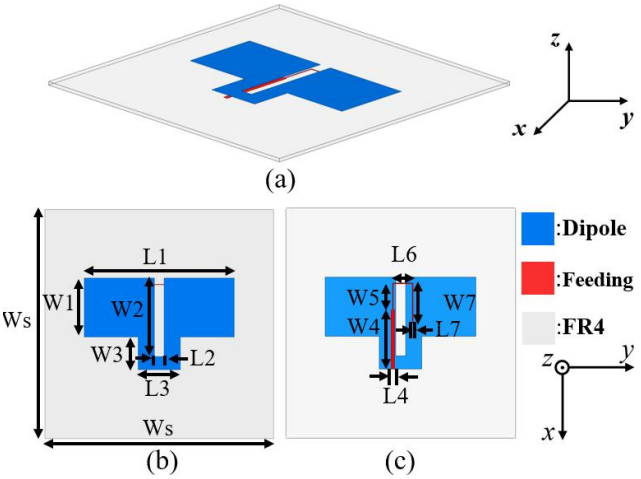

FIGURE 1. Geometry of the proposed dipole antenna. (a) 3D view. (b) and (c) Top and back view.

TABLE I. Dimensional parameters of the proposed dipole antennas

Parameters	Values(mm)	Parameters	Values(mm)
Ws	70	L1	46
W1	18	L2	3
W2	24	L3	13
W3	10	L4	1
W4	18	L6	6.3
W5	8	L7	0.2
W7	11.9		

As shown in Figure 2, Although the initial dipole antenna has the −10 dB impedance bandwidth (BW) of 88.5% (2.16–4.33 GHz), with a low peak gain of only 2.04 dBi and poor maximum FBR of 1.03 dB, achieving omnidirectional radiation, as shown in Figure 3. However, the antenna exhibit AR greater than 3 dB, indicating LP radiation.

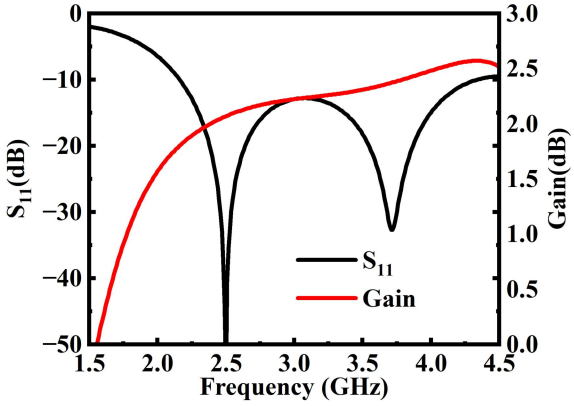

FIGURE 2. Simulated results of the proposed dipole antenna.

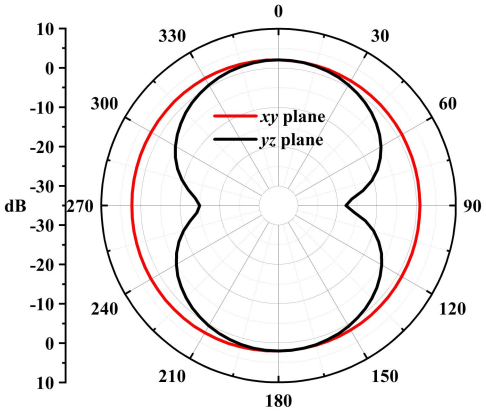

FIGURE 3. Simulated normalized radiation pattern of the proposed dipole antenna at 2.45 GHz.

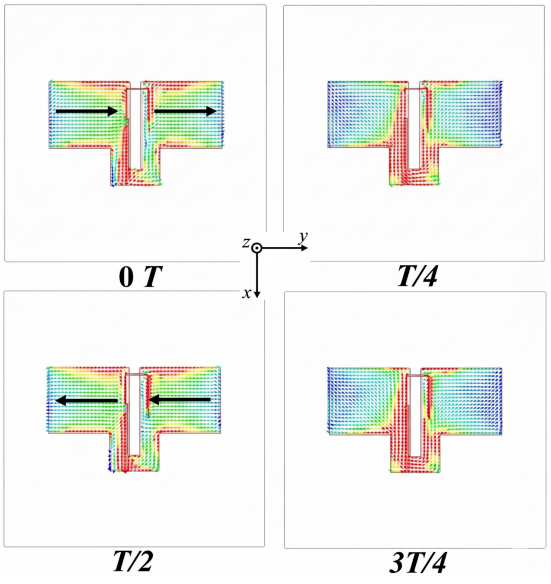

FIGURE 4. Simulated surface current distributions of the proposed dipole antenna at 2.45 GHz.

Figure 4 illustrates the surface current distribution of the dipole antenna at 2.45 GHz, respectively. At t=0 and T/2, the

current flows uniformly along the dipole arms in the $+y$ and $-y$ directions, respectively, while the current on the segmented ring is minimal. Conversely, at t=T/4 and 3T/4, while the dipole current is minimal.

III. DESIGN AND ANALYSIS OF CP DIPOLE ANTENNA WITH PRAMC

A. Polarization Rotation Mechanism of PRAMC

To clarify the polarization rotation principle of PRAMC, we consider the PRAMC lies in the *xoy* plane, as shown in Figure 5. An incident wave propagates along the $-z$ direction and can be decomposed into two orthogonal components of E_x and E_y.

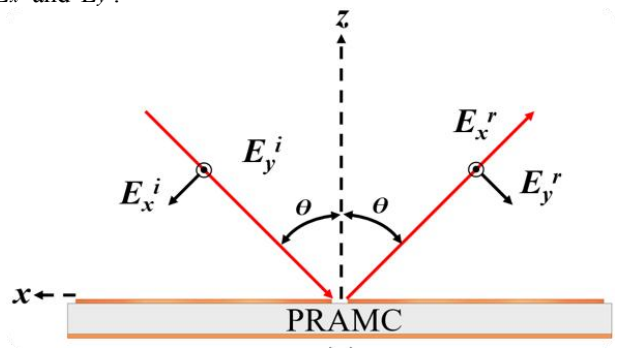

FIGURE 5. Polarization rotation mechanism of PRAMC.

When the PRAMC is illuminated by the incident wave $\vec{E}^i$, it generates a reflected wave $\vec{E}^r$. The relationship between them can be expressed as [17]

$$\vec{E}^r = \overline{\overline{\Gamma}} \times \vec{E}^i \tag{1}$$

where $\overline{\overline{\Gamma}}$ is dyadic reflection coefficient, which can be given as

$$\overline{\overline{\Gamma}} = \begin{bmatrix} \Gamma xx & \Gamma xy \\ \Gamma yx & \Gamma yy \end{bmatrix} \tag{2}$$

Here, Γ_{yx} is a key parameter for polarization conversion, measuring the efficiency of converting x-polarized incident waves into y-polarized reflected waves.

Assuming the antenna radiates along the $+z$ direction and the incident wave onto the PRAMC surface is x-polarized, the $\vec{E}^i$ can be expressed as

$$\vec{E}^i = E_0 \cdot \hat{x} \cdot e^{-jk_0 z} \tag{3}$$

Therefore, the total radiation field can be calculated as

$$\begin{aligned} \vec{E}^{total} &= \vec{E}^i + \vec{E}^r = (1+\overline{\overline{\Gamma}})\vec{E}^i \\ &= E_0 \cdot e^{-jk_0 z}((1+|\Gamma xx| \cdot e^{-j\theta xx}) \cdot \hat{x} \\ &\quad + |\Gamma yx| \cdot e^{-j\theta yx} \cdot \hat{y}) \end{aligned} \tag{4}$$

where $|\Gamma xx|$ and $|\Gamma yx|$ are the magnitudes, θxx and θyx are the phases. The $\vec{E}^{total}$ can be decomposed into two CP components of E_R and E_L. Thus, the AR can be calculated as

$$AR(dB) = 20\log\left(\frac{|E_R|+|E_L|}{|E_R|-|E_L|}\right) \tag{5}$$

The polarization conversion ratio (PCR) of a PRAMC can characterize its ability to convert incident waves into orthogonally polarized waves. It can be calculated using the magnitudes of the two reflection coefficients $|\Gamma xx|$ and $|\Gamma yx|$, with the formula:

$$PCR = |\Gamma xx|^2 \Big/ \left(|\Gamma xx|^2 + |\Gamma yx|^2\right) \tag{6}$$

B. DESIGN AND ANALYSIS OF PRAMC UNIT

Figure 6 shows the evolution from ring-shaped AMC to segmented ring-shaped PRAMC, the reflection characteristics of two are analyzed using the Floquet-port model in ANSYS HFSS, with detailed dimensions provided in Table 2.

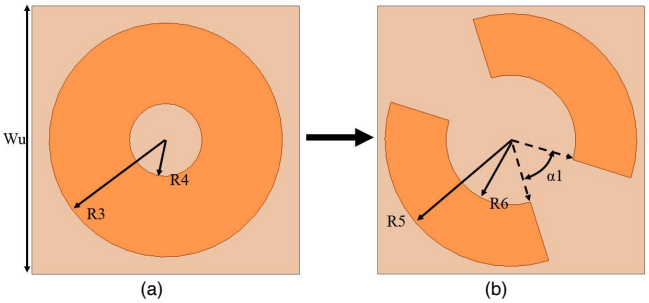

FIGURE 6. The evolution from AMC to PRAMC. (a) AMC unit. (b) PRAMC unit.

The underlying mechanism of the 90 ° phase difference introduced by corner truncation can be physically interpreted as follows. The intact ring-shaped AMC exhibits perfect symmetry with respect to the *x*- and *y*-axes, resulting in identical equivalent impedances along the two orthogonal directions and thus a 0 ° reflection phase difference. By truncating the four corners along the 45° direction, the structural symmetry is broken, introducing orthogonal anisotropy. In terms of the equivalent circuit model, the corner truncation effectively introduces additional series capacitances at the corners, which alter the equivalent inductance-capacitance products along the two principal axes. Consequently, an incident *x*-polarized wave is decomposed into two orthogonal components that experience distinct phase delays. When the truncation angle is optimally chosen, the phase difference between these two components reaches 90°, satisfying the condition for left-hand circular polarization (LHCP) radiation. This is further verified by the surface current distribution in Figure 10, where the rotated and phase-shifted currents confirm the polarization conversion mechanism. Physically, the corner truncation introduces anisotropic boundary conditions that perturb the diagonal reflection coefficients (Γxx and Γyx) and, more

importantly, significantly excite the cross-polarization term (Γ_{yx}). The optimal truncation maximizes Γ_{yx} while enforcing $\theta_{yy} - \theta_{xx} = 90^0$, which is precisely the condition quantified by the PCR in (6).

As shown in Figure 7(a), the ±90° in-phase reflection phase bandwidth of the AMC unit is 130 MHz (2.38–2.51 GHz), and the resonant frequency corresponding to the midpoint of the phase range at 0° is 2.45 GHz. The conversion from the AMC with 0° phase difference to PRAMC with 90° phase difference is achieved through corner truncation of AMC along the 45° direction, as shown in Figure 7(a). At the center frequency of 2.45 GHz, an x-polarized incident wave is efficiently converted into a y-polarized reflected wave, and the phase of the y-polarized reflected wave leads that of the x-polarized incident wave by +90°, satisfying the condition for forming a LHCP wave. Within the frequency range of 150 MHz (2.38–2.53 GHz), the x-polarized reflected wave is suppressed, while the y-polarized is strongly excited, with 90° phase difference, achieving the PCR exceeding 90%, as shown in Figure 7(b).

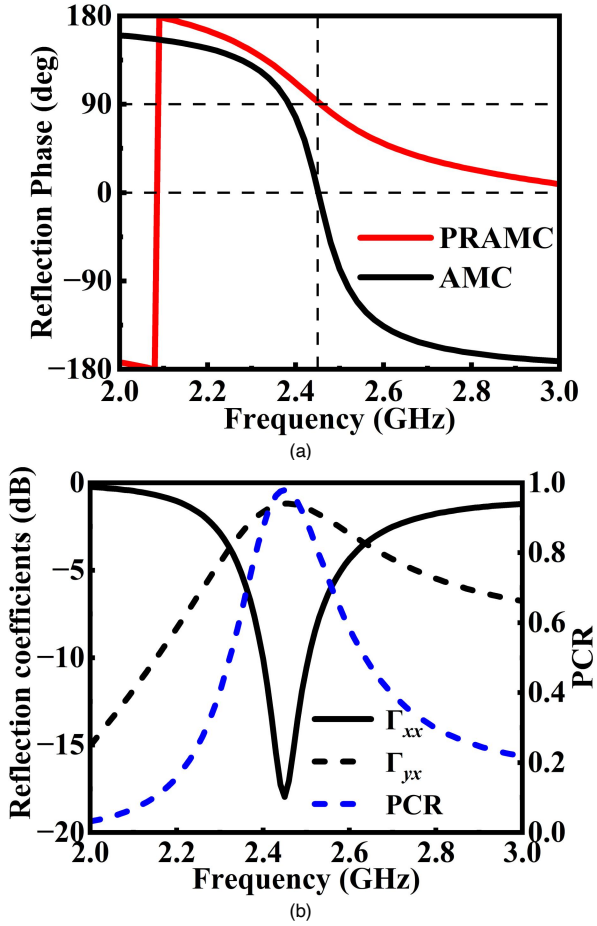

FIGURE 7. (a) The reflection phase change from the AMC unit to the PRAMC unit. (b) Reflection coefficients and PCR of the PRAMC unit.

C. DESIGN AND ANALYSIS OF CP DIPOLE ANTENNA WITH PRAMC

In order to verify that PRAMC can convert the LP radiation of an electric dipole into CP radiation, the schematic diagram of the antenna structure transitioning from a LP dipole loaded with AMC to a CP dipole loaded with PRAMC is shown in Figure 8, with detailed dimensions provided in Table II. First, a 2×2 ring-shaped AMC array with the same area as the dipole antenna is loaded beneath the antenna as a reflector to enhance the gain. Furthermore, a 2×2 segmented ring-shaped PRAMC array is employed to replace the original AMC array, serving as a polarization rotation reflector. This configuration not only improves the antenna gain but also achieves polarization conversion.

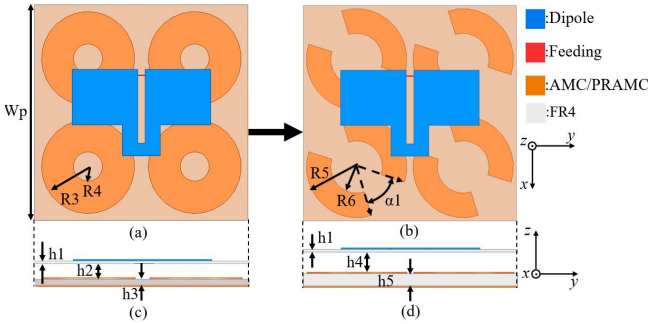

FIGURE 8. (a) and (c) Top and side views of LP dipole antenna with AMC. (b) and (d) Top and side views of CP dipole antenna with PRAMC.

TABLE II. Dimensional Parameters of the Proposed Antennas, AMC and PRAMC Unit

Parameters	Values(mm)	Parameters	Values(mm)
Wp	70	h5	4
Wu	35	R3	15.25
h1	0.8	R4	4.75
h2	6	R5	16.5
h3	2	R6	8.5
h4	7	α1	55 deg

The simulated results of the dipole antenna loaded with AMC are shown in Figure 14. The antenna operates at 2.45 GHz, with a −10 dB impedance BW of 5.3% (2.40–2.53 GHz). The peak gain is further increased to 6.1 dBi, achieving directional radiation, as shown in Figure 9(a). However, the antenna with AMC still exhibits AR greater than 3 dB, indicating LP radiation.

Moreover, the simulated results of the final proposed CP dipole antenna with PRAMC shows the −10 dB impedance BW of 45.3% (2.19–3.30 GHz), the AR BW of 3.7% (2.40–2.49 GHz), with the peak gains of 7.73 dBi, as shown in Figure 14. The simulated radiation patterns at 2.45 GHz show the co-polarized LHCP gain of 6.55 dBi, the cross-polarized RHCP gain of −18.1 dBi along the main beam direction in the *xz* and *yz* planes, respectively, as shown in Figure 9(b). This validates that the 90° phase difference introduced by the PRAMC generates the LHCP radiation.

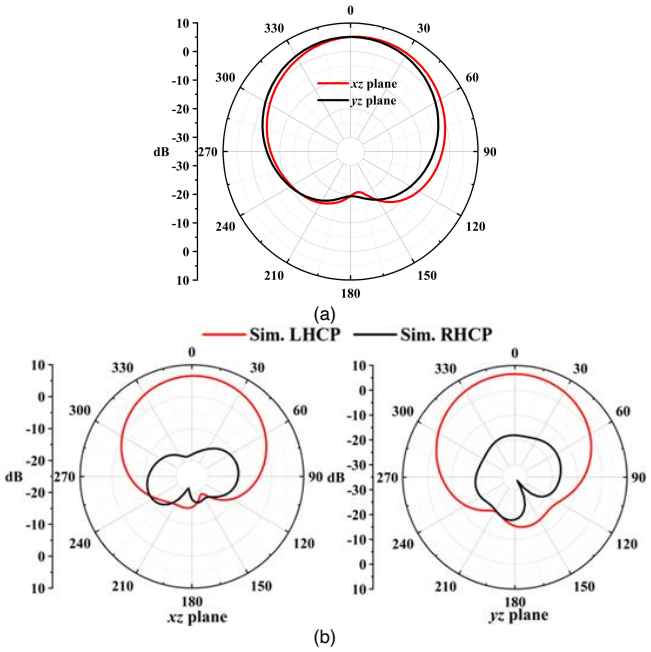

FIGURE 9. (a) dipole antenna with AMC. (b) CP dipole antenna with PRAMC.

Figure 10 further shows the surface current distribution of the dipole antenna loaded with PRAMC at 2.45 GHz at different moments within one complete operating cycle. It can be observed from the figure that at t=0 and t=T/2, the surface current mainly flows uniformly along the two arms of the dipole in the +*y* and −*y* directions, respectively, while the current on the PRAMC surface is relatively weak. In contrast, at t=T/4 and t=3T/4, the current is primarily distributed on the PRAMC surface, flowing in the +45° and −45° directions, respectively, while the current on the dipole surface decreases to a minimum.

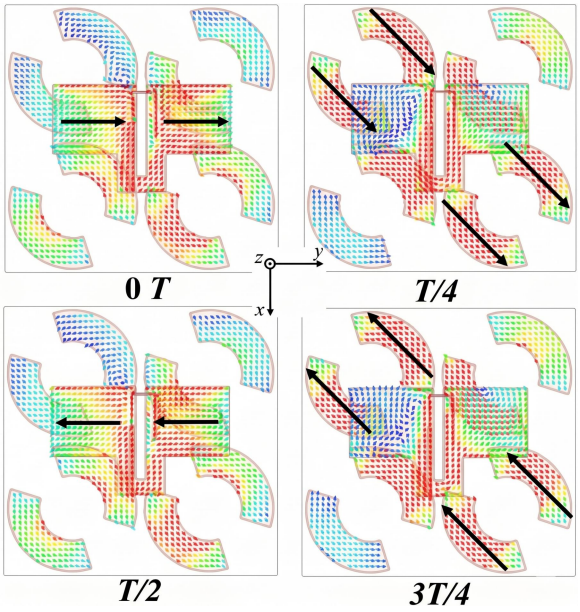

FIGURE 10. Simulated surface current distributions of the proposed CP dipole antenna with PRAMC at 2.45 GHz.

According to the IEEE definition, when viewed along the +*z* direction, the current variation over the entire cycle reveals that as the phase changes, the composite current rotates in a clockwise direction. The introduction of PRAMC enables the originally linearly polarized dipole antenna to achieve LHCP radiation through the redistribution and phase control of surface currents.

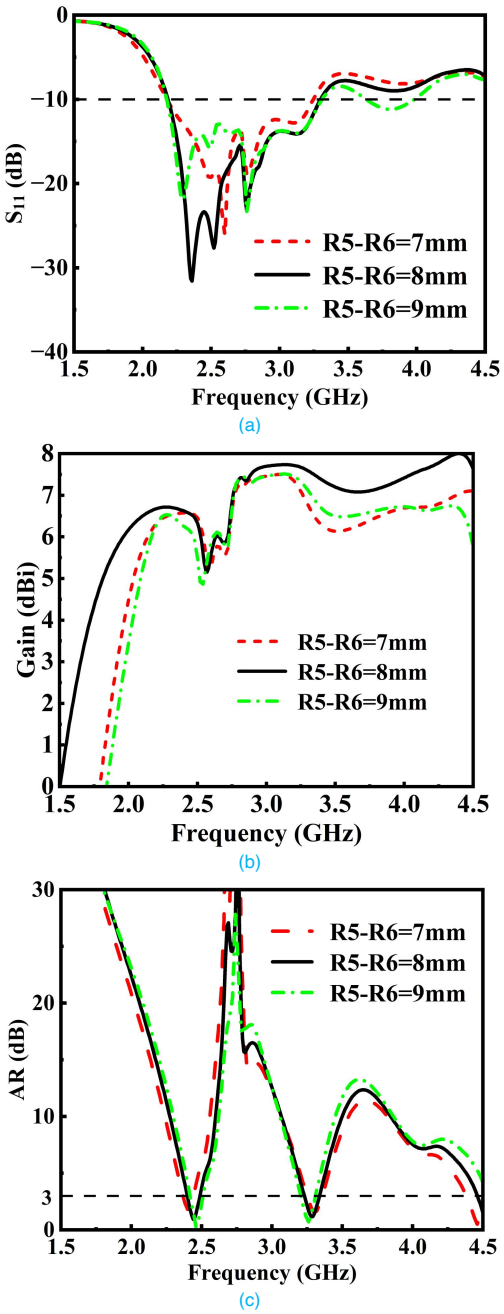

FIGURE 11. Simulated (a) S_{11}, (b) gain and (c) AR of the proposed dipole antenna with PRAMC for different values of the segmented-ring width R5-R6.

To provide a clearer understanding of the antenna design evolution, a parametric study is conducted on the simulation model to investigate the influence of the segmented-ring width R5-R6, the truncation angle α1, and the spacing h4

between the PRAMC array and the dipole on the S_{11}, gain, and AR, with the results presented in Figure 11, 12, and 13, respectively.

As shown in Figure 11, as the segmented-ring width R5-R6 increases, the center frequency of the antenna gradually shifts toward lower frequencies. This is because a wider ring increases the equivalent inductance and capacitance of the PRAMC unit, thereby lowering its resonant frequency.

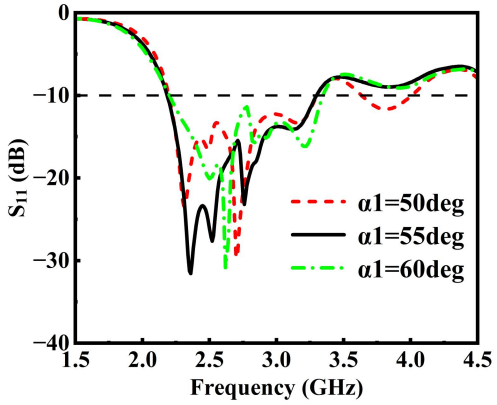

(a)

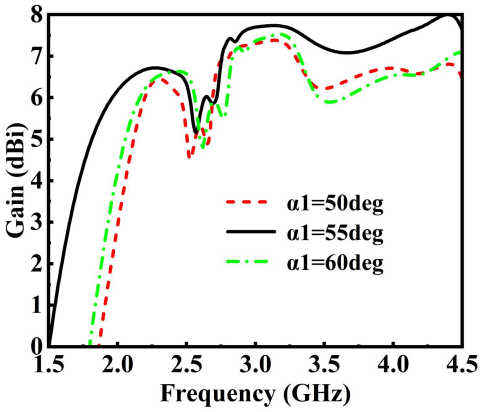

(b)

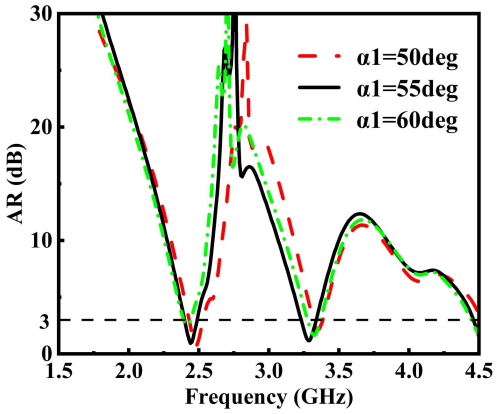

(c)

FIGURE 12. Simulated (a) S_{11}, (b) gain and (c) AR of the proposed dipole antenna with PRAMC for different values of the truncation angle α1.

Moreover, as shown in Figure 12, with the increase of the truncation angle α1 the center frequency of the antenna shifts toward higher frequencies. This is because a larger truncation angle introduces stronger capacitive loading at the corners of the segmented ring, which reduces the equivalent inductance and raises the resonant frequency of the PRAMC unit. Meanwhile, both the gain and axial ratio are also enhanced with increasing α1, since a more pronounced corner truncation improves the orthogonal phase difference and polarization conversion efficiency.

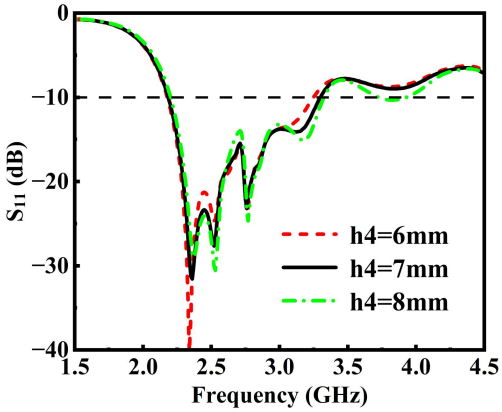

(a)

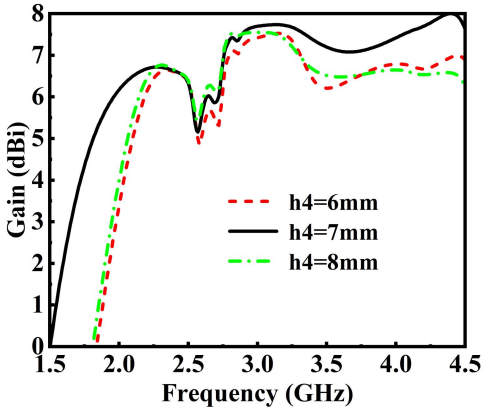

(b)

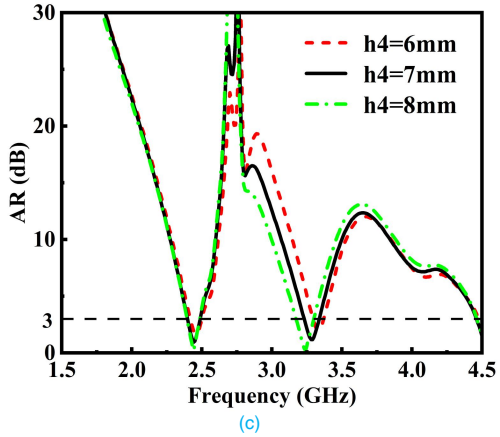

(c)

FIGURE 13. Simulated (a) S_{11}, (b) gain and (c) AR of the proposed dipole antenna with PRAMC for different values of the spacing h4 between the PRAMC array and the dipole.

Finally, as shown in Figure 13, the center frequency and gain of the antenna are nearly insensitive to the variation of the dipole-to-PRAMC distance. In contrast, the axial ratio is

found to decrease and improve with increasing h4, indicating that a larger spacing enhances the phase difference precision between the two orthogonal components. This improvement can be attributed to the reduced mutual coupling and parasitic effects at a larger separation, which allows the PRAMC to more effectively perform its polarization rotation function.

The parametric study yields the following design guidelines. The width R5-R6 mainly controls frequency tuning with little effect on gain and AR. The truncation angle α1 requires careful optimization to maintain the 90° phase condition for CP radiation. The spacing h4 should be minimized for low profile and strong coupling, yet sufficiently large to avoid AR degradation. Accordingly, the optimal parameters are determined as R5-R6 = 8 mm, α1 = 55 deg and h4 = 7 mm, which are adopted in the final design.

D. ANTENNAS PERFORMANCE ANALYSIS

Figure 14 shows the simulated performance comparison of the different designed dipole antennas. Table III summarizes and compares the performance of the antennas, which the evolution of the dipole antenna performance from LP to CP. Compared with the single dipole antenna and the dipole antenna loaded with the AMC, the dipole antenna loaded with the PRAMC achieves peak gain improvements of 5.69 dBi and 1.62 dBi, respectively, while maintaining the same operating frequency of 2.45 GHz. Moreover, it exhibits an axial ratio bandwidth of less than 3 dB that covers the 2.45 GHz ISM band. Further, by comparing the simulation results

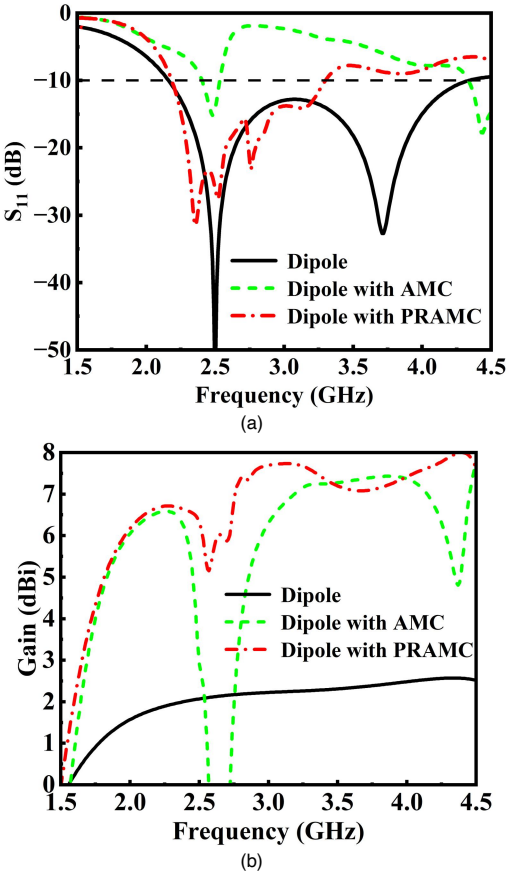

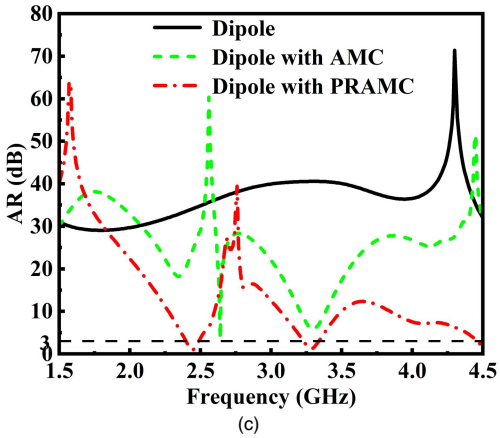

FIGURE 14. Simulated performance comparison of the proposed different antennas. (a)S_{11}. (b) Gain. (c) AR.

of the dipole antenna loaded with the AMC and that loaded with the PRAMC, it is found that the AMC array only improves the gain of the dipole antenna. Significantly, the most notable distinction of the PRAMC-loaded design is that it not only achieves gain enhancement but also accomplishes a polarization conversion from LP to LHCP, realizing a planar CP dipole antenna for the 2.45 GHz ISM band.

TABLE III. Simulated Performances Comparison of the Proposed Different Antennas

Antenna Type	f_0 (GHz)	−10 dB Impedance BW	Peak Gain (dBi)	Polarization
Dipole	2.45	88.5% (2.16–4.34 GHz)	2.04	LP
Dipole with AMC	2.45	5.3% (2.40–2.53 GHz)	6.1	LP
Dipole with PRAMC	2.45	45.3% (2.19–3.30 GHz)	7.73	CP

IV. ANTENNA FABRICATION AND MEASUREMENT

Figure 15 shows the CP dipole antenna with PRAMC prototype was fabricated and measured to validate the simulated results. The return loss S_{11} of the proposed antenna is measured using a vector network analyzer (VNA). The far-field radiation characteristics are measured in anechoic chamber (AC). The measured results are presented in Figure 16 and 17.

As shown in Figure 16, the simulated and measured results of the final proposed CP dipole antenna with PRAMC shows the −10 dB impedance BWs of 45.3% (2.19–3.30 GHz) and 29.8% (2.21–2.94 GHz), the AR BWs of 3.7% (2.40–2.49 GHz) and 7% (2.35–2.52 GHz), with the peak gains of 7.73 dBi and 7.01 dBi, respectively, achieving CP radiation. As shown in Figure 17, the radiation patterns the proposed CP dipole antenna with PRAMC at 2.45 GHz show the simulated and measured co-polarized left-hand CP (LHCP) gain of 6.55 dBi and 6.33 dBi, the cross-polarized right-hand CP (RHCP) gains of −18.1 dBi and −16.42 dBi along the

main beam direction in the *xz* and *yz* planes, respectively. This validates that the 90° phase difference introduced by the PRAMC generates the LHCP radiation.

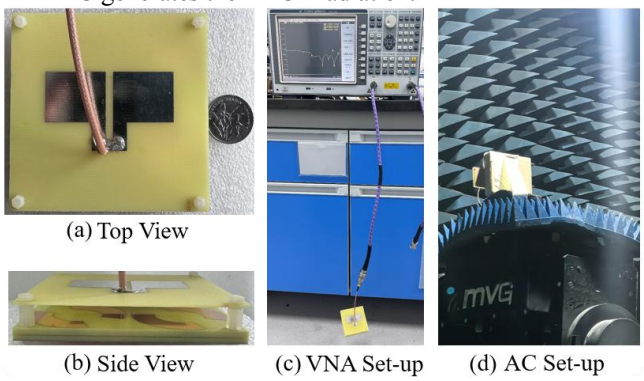

FIGURE 15. (a) and (b) Top and side view of the fabricated CP dipole antenna with PRAMC. (c) S11 measurement setup using the VNA. (d) Radiation pattern measurement setup in the AC.

Finally, by comparing the simulated and measured results of the antenna, it can be observed that the 90° phase difference introduced by the PRAMC effectively enables the conversion of the dipole antenna from LP to LHCP. Overall, the measured results are in good agreement with the simulated results, validating the feasibility of the proposed design method. Although the measured −10 dB impedance bandwidth is somewhat narrower than the simulated one, this discrepancy is mainly attributed to the following factors:

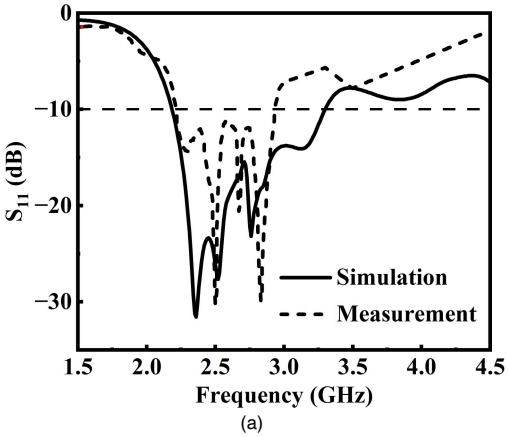

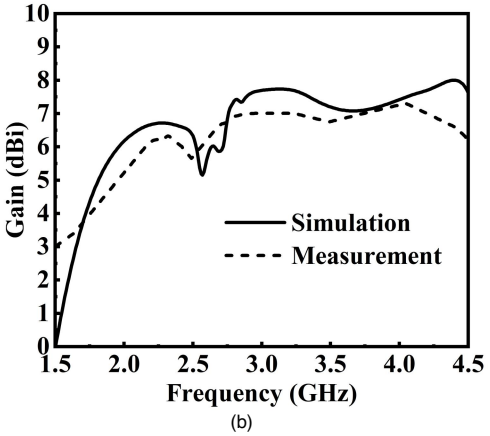

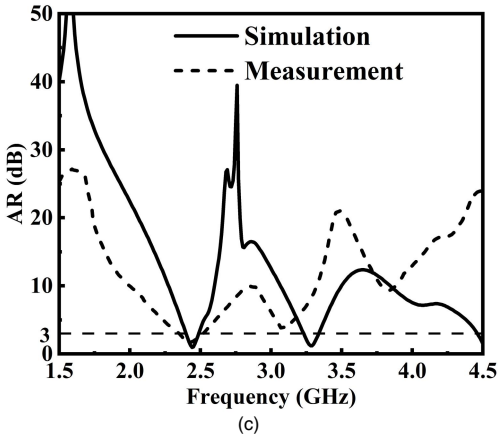

FIGURE 16. Simulated and measured performance of the proposed CP dipole antenna with PRAMC. (a) S11. (b) Gain. (c) AR.

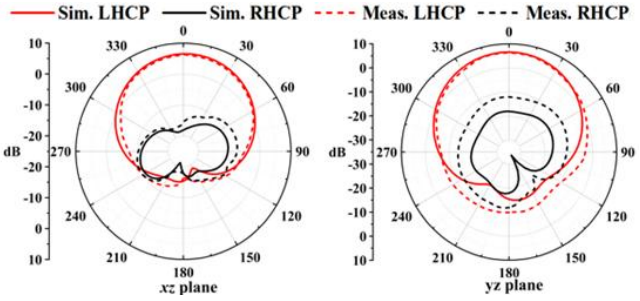

FIGURE 17. Simulated and measured normalized radiation patterns of the proposed CP dipole antenna with PRAMC at 2.45 GHz.

fabrication errors, including deviations between the actual values of the dielectric constant and loss tangent of the FR4 substrate and those set in the simulation; uncertainties in the soldering process, particularly the influence of the soldering quality between the L-shaped balun feed line and the coaxial connector on impedance matching; and parasitic effects in the measurement environment.

Table IV gives a comparison of the overall performance of the proposed CP dipole antenna with other works at 2.45 GHz ISM band, where λ_0 indicates the wavelength in free space's center frequency at 2.45 GHz. In Refs. [9]–[12], conventional CP dipole antennas are primarily based on the complementary principle of electric and magnetic dipoles to achieve high gain and CP radiation. However, these designs are often accompanied by issues such as complex structures, cumbersome fabrication processes, and relatively narrow −10 dB impedance bandwidth and 3 dB axial ratio bandwidth in the 2.45 GHz ISM band, as well as limited gain performance. Furthermore, although the CP antenna proposed in Ref. [16] improves gain by loading AMC, its impedance and AR BWs remain narrow. Similarly, in Refs. [18] and [19], CP antennas employing Polarization-Converting Metasurface (PCMS) to achieve polarization conversion still fail to obtain significant improvement in impedance and AR BWs. Compared to the previous design of the CP dipole antennas operating at the 2.45 GHz ISM band, the proposed CP dipole antenna has a relatively higher gain and wider −10 dB impedance BW and

3 dB AR BW at the 2.45 GHz ISM band. Furthermore, compared with the other dipole antennas designed in this paper, a significant gain enhancement and a conversion from LP to LHCP are achieved.

TABLE IV. Comparison Between the Proposed CP Dipole Antenna and Other Works

Ref.	f_0 (GHz)	CP Method	Peak Gain (dBic)	−10 dB Impedance BW (%)	3 dB AR BW (%)
[9]	2.45	Cross-dipoles	7.7	21.2	2.9
[10]	2.45	Cross-dipoles	4	8.98	6.93
[11]	2.45	SIW	0.87	4.08	5.76
[12]	2.45	ME-dipole	1.6	6.7	8.4
[16]	2.45	Patch + AMC	6.05	1.96	2.0
[18]	2.45	Monopole + PCMS	6.5	20.8	2.65
[19]	2.45	Monopole + MS	6.5	14.7	5.3
Prop.	2.45	Dipole + PRAMC	7.01	29.8	7.0

V. CONCLUSION

In this paper, a planar CP dipole antenna based on PRAMC operating at 2.45 GHz ISM band has been proposed. The design demonstrates that a PRAMC can serve as a dual-function reflector that simultaneously provides gain enhancement and orthogonal phase manipulation for LP-to-CP conversion. The measured results show that the proposed antenna has the −10 dB impedance BW of 29.8% (2.21–2.94 GHz) and AR BW of 7.0% (2.35–2.52 GHz), with a peak gain of 7.01 dBi. This results effectively demonstrate that the PRAMC can convert a low-gain LP dipole antenna into a high-gain CP dipole antenna. The proposed PRAMC-based design strategy offers a promising pathway for developing low-cost, high-performance planar CP dipole antennas in ISM-band applications."

ACKNOWLEDGMENT

This work was supported in part by National Natural Science Foundation of China (62565012), the Yunnan Provincial Foundation Program (Grant No. 202501AS070048), the Yunnan Fundamental Research Projects (Grant No. 202301BE070001-005), Innovation Capability Support Program of Shaanxi (Program No.2025QCY-KXJ-041), and Jiangsu Province Deputy General Manager of Science and Technology (Program No. FZ20240945).

REFERENCES

[1] Q. -Q. He, B. -Z. Wang and J. He, "Wideband and Dual-Band Design of a Printed Dipole Antenna," in *IEEE Antennas and Wireless Propagation Letters*, vol. 7, pp. 1-4, 2008, doi: 10.1109/LAWP.2007.913325.

[2] L. Kuo, H.-R. Chuang, Y.-C. Kan, T. S. Huang, and Che Ming Ko, "A Study of Planar Printed Dipole Antennas for Wireless Communication Applications," in *Journal of Electromagnetic Waves and Applications*, vol. 21, no. 5, pp. 637–652, Jan. 2007, doi: 10.1163/156939307780667355.

[3] R. -C. Hua and T. -G. Ma, "A Printed Dipole Antenna for Ultra High Frequency (UHF) Radio Frequency Identification (RFID) Handheld Reader," in *IEEE Transactions on Antennas and Propagation*, vol. 55, no. 12, pp. 3742-3745, Dec. 2007, doi: 10.1109/TAP.2007.910521.

[4] J Lei, G Fu, L Yang, et al., "An omnidirectional printed dipole array antenna with shaped radiation pattern in the elevation plane," *Journal of Electromagnetic Waves and Applications*, vol. 20, no. 14, pp. 1955-1966, 2006. doi: 10.1163/156939306779322639

[5] N. Hussain et al., "A Compact Flexible Frequency Reconfigurable Antenna for Heterogeneous Applications," in *IEEE Access*, vol. 8, pp. 173298-173307, 2020, doi: 10.1109/ACCESS.2020.3024859.

[6] X. Yang, Y. Liu and S. -X. Gong, "Design of a Wideband Omnidirectional Antenna With Characteristic Mode Analysis," in *IEEE Antennas and Wireless Propagation Letters*, vol. 17, no. 6, pp. 993-997, June 2018, doi: 10.1109/LAWP.2018.2828883.

[7] M. Farahani, M. Akbari, M. Nedil, A. -R. Sebak and T. A. Denidni, "Millimeter-Wave Dual Left/Right-Hand Circularly Polarized Beamforming Network," in *IEEE Transactions on Antennas and Propagation*, vol. 68, no. 8, pp. 6118-6127, Aug. 2020, doi: 10.1109/TAP.2020.2986678.

[8] Y. Yin and K. Wu, "Endfire Circularly Polarized Planar Antennas: A review of their development," in *IEEE Antennas and Propagation Magazine*, vol. 65, no. 2, pp. 63-75, April 2023, doi: 10.1109/MAP.2022.3154977.

[9] T T Le, H H Tran., "Dual-band dual-sense circularly polarized antenna based on crossed dipole structure for WLAN/WiMAX applications," *International Journal of RF and Microwave Computer-Aided Engineering*, vol. 29, no. 10, pp. e21866, Oct. 2019, doi: 10.1002/mmce.21866.

[10] C Bajaj, D K Upadhyay, S Kumar, et al. "Compact Circularly Polarized 2.45/5.8-GHz Antenna for RFID Readers," in 2021 *IEEE International Conference on RFID Technology and Applications (RFID-TA)*. IEEE, 2021, pp. 63-66, doi: 10.1109/RFID-TA53372.2021.9617345.

[11] S S Gu, W J Lu, L Zhu, "2D sectorial dipole-enabled planar endfire circularly polarized antenna with widened azimuth half-power beamwidth," *Electronics Letters*, vol. 60, no. 14, pp. e13301, 2024, doi: 10.1049/ell2.13301.

[12] J L Guo, C Li, Y H Yang, et al., "Low-profile omnidirectional circularly polarized antenna based on substrate integrated waveguide technology," *International Journal of RF and Microwave Computer-Aided Engineering*, vol. 28, no. 6, pp. e21289, Aug. 2018, doi: 10.1002/mmce.21289.

[13] S. Kim, Y. -J. Ren, H. Lee, A. Rida, S. Nikolaou and M. M. Tentzeris, "Monopole Antenna With Inkjet-Printed EBG Array on Paper Substrate for Wearable Applications," in *IEEE Antennas and Wireless Propagation Letters*, vol. 11, pp. 663-666, 2012, doi: 10.1109/LAWP.2012.2203291.

[14] A. Y. I. Ashyap et al., "An Overview of Electromagnetic

Band-Gap Integrated Wearable Antennas," in *IEEE Access*, vol. 8, pp. 7641-7658, 2020, doi: 10.1109/ACCESS.2020.2963997.

[15] W. Yang, W. Che, H. Jin, W. Feng and Q. Xue, "A Polarization-Reconfigurable Dipole Antenna Using Polarization Rotation AMC Structure," in *IEEE Transactions on Antennas and Propagation*, vol. 63, no. 12, pp. 5305-5315, Dec. 2015, doi: 10.1109/TAP.2015.2490250.

[16] S. Sarkar and B. Gupta, "A Dual-Band Circularly Polarized Antenna With a Dual-Band AMC Reflector for RFID Readers," in *IEEE Antennas and Wireless Propagation Letters*, vol. 19, no. 5, pp. 796-800, May 2020, doi: 10.1109/LAWP.2020.2980325.

[17] H. Yang, X. Liu, Y. Fan and L. Xiong, "Dual-Band Textile Antenna With Dual Circular Polarizations Using Polarization Rotation AMC for Off-Body Communications," in *IEEE Transactions on Antennas and Propagation*, vol. 70, no. 6, pp. 4189-4199, June 2022, doi: 10.1109/TAP.2021.3138504.

[18] N. K. Sahu and S. K. Mishra, "Polarization-Converting Metasurface Inspired Dual-Band Dual-Circularly Polarized Monopole Antennas for Off-Body Communications," in *IEEE Antennas and Wireless Propagation Letters*, vol. 22, no. 1, pp. 194-198, Jan. 2023, doi: 10.1109/LAWP.2022.3206913.

[19] N. K. Sahu and S. K. Mishra, "Compact Dual-Band Dual-Polarized Monopole Antennas Using Via-Free Metasurfaces for Off-Body Communications," in *IEEE Antennas and Wireless Propagation Letters*, vol. 21, no. 7, pp. 1358-1362, July 2022, doi: 10.1109/LAWP.2022.3167849.

[20] Y Zhu, H Chen, L Li, et al. "A novel planar broadband end-fire antenna with high front-to-back ratio." *Progress in Electromagnetics Research Letter*, vol. 109, pp. 85-92, Mar. 2023, doi: 10.2528/PIERL22122604.

[21] X Yang, Y Zhu, Q Wang, et al. "Bandwidth reconfigurable wideband electromagnetic dipole complementary end-fire antenna based on VO2 switch, " *Journal of Electromagnetic Waves and Applications*, vol. 40, no. 5, pp. 795-807, 2026, doi: 10.1080/09205071.2025.2609147.